A METHOD BASED ON EXPLICIT GRADIENT RECONSTRUCTION APPLIED TO PETROLEUM RESERVOIR SIMULATION

Giovani Cerbato

giovani.cerbato@sinmec.ufsc.br

Gustavo Gondran Ribeiro

ggrbill@sinmec.ufsc.br

Fernando S. V. Hurtado

fernando@sinmec.ufsc.br

Clovis R. Maliska

maliska@sinmec.ufsc.br

António Fábio Carvalho da Silva

afabio@sinmec.ufsc.br

Federal University of Santa Catarina, Department of Mechanical Engineering, SINMEC Laboratory, 88040-900, Florianópolis, Santa Catarina, Brasil.

Abstract. *Polyhedral grids are a kind of unstructured grids whose use in petroleum reservoir simulation is attractive for discretizing geometrically complex reservoirs. The present work focuses on the analysis of a discretization method able to deal with those grids. The methodology is a finite volume method with fluxes approximated using a scheme here called "corrected two-point flux approximation" (CTPFA). In this scheme, the flux expression is written as the sum of two terms. The first one is an implicit term involving only two points, similar to the approximation used in conventional methods applied to corner-point grids. The second term is a correction term, in which the effects of anisotropy and non-orthogonality are included. This term is expressed using gradient values associated with the control volumes that share a given face. The gradients are approximated by gradient reconstruction methods that employ discrete pressure values of a previous level of iteration. It is clear that an iterative process is necessary in order to obtain a numerical solution of a differential equation. Test problems are presented in order to analyze the behavior of discretization error associated to the present methodology.*

Keywords: *Polyhedral grids, finite volume method, petroleum reservoir simulation*

1 INTRODUCTION

Unstructured grids can represent complex geometries in an accurate and efficient way. They are extensively employed in numerical simulation of physical problems in different areas, like fluid dynamics and structural analysis. In petroleum reservoir simulation the corner-point grids, a type of structured grids, are the *de facto* standard for the discrete representation of petroleum reservoirs geometry in commercial simulators. However, in some cases, those grids lack geometrical flexibility for representing adequately intricate geological features. In such cases polyhedral grids are an attractive alternative because of their intrinsic flexibility. Moreover, polyhedral grids have comparatively less cells than a conventional unstructured grid, especially a tetrahedral one, for the same refinement level.

In order to employ polyhedral grids in reservoir simulation, it is necessary to develop methodologies suitable to handle them and, at a same time, to treat adequately the reservoir flow model intricacies. A possible alternative, based on explicit gradient reconstruction, is presented in this work. It is a conventional cell-centered finite volume method whose distinctive feature is the approximation of diffusive fluxes on the faces of a polyhedral grid through the so-called "corrected two-point flux approximation" (CTPFA). In this scheme, the flux expression is written as the sum of two terms. The first one is similar to the flux expression used in conventional methods in reservoir simulation, including only two pressure discrete values. The second term, which can be considered a correction term, takes into account non-orthogonality and anisotropy. Since this correction term usually involves a large set of pressure values, in this work, it is treated explicitly.

1.1 Polyhedral grids

Polyhedral grids can be defined as a finite portion of a region in the three-dimensional space that is composed by polyhedral cells, limited by an arbitrary number of faces. Those cells should fill completely the region where the grid is defined, in order to avoid empty spaces inside it. Each face of a polyhedral cell is a polygon composed by an arbitrary number of sides. Polyhedral cells and polygonal faces are entities that form polyhedral grids, as well as the edges and the vertices. An example of a polyhedral grid can be seen in section 3 and an illustration of the main entities is shown in Fig. 1.

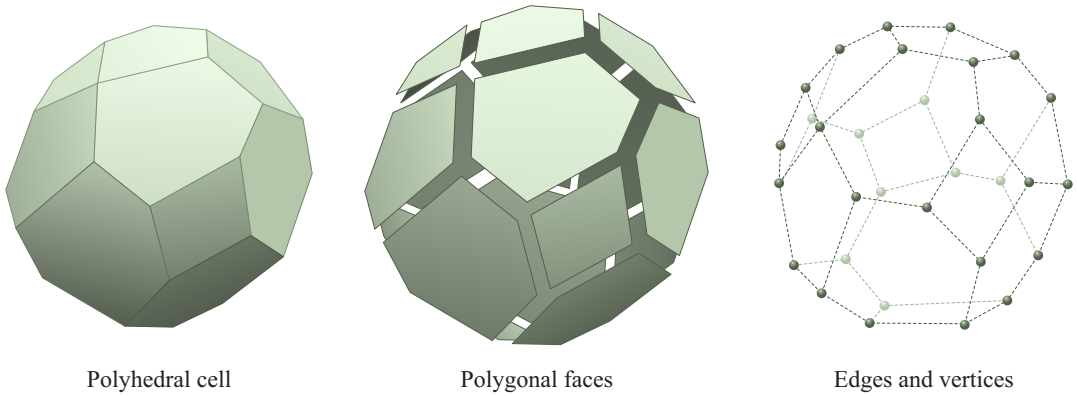

Figure 1: Geometric entities in a polyhedral grid. Modified from Maliska et al. (2012b).

1.2 Fluid flow model

In order to describe the proposed numerical methodology, an incompressible single-phase model is considered in this work. The differential equation that models the pressure variation in this type of flow is the elliptic equation

$$-\boldsymbol{\nabla}\cdot\mathbf{K}\cdot\boldsymbol{\nabla}P = f\,, \tag{1}$$

where $\mathbf{K}$ is the permeability tensor, a second order symmetric and positive-definite tensor, P is the pressure and f is the source term. Although this is a simple flow model, more complex flow models in reservoir simulation always involve the term $-\boldsymbol{\nabla}\cdot\mathbf{K}\cdot\boldsymbol{\nabla}P$, or a variant of it. One of the major difficulties in any reservoir flow model is precisely the discretization of that term.

Considering the integration of Eq. (1) over a polyhedral control volume $\mathcal{V}_\mathsf{p}$, the resulting equation is

$$-\sum_{k=1}^{N_f}\int_{\mathsf{f}_k}\mathbf{K}\cdot\boldsymbol{\nabla}P\cdot\mathrm{d}\mathbf{S} = \int_{\mathcal{V}_\mathsf{p}} f\,\mathrm{d}V\,, \tag{2}$$

where N_f is the number of faces f_k that delimits the control volume $\mathcal{V}_\mathsf{p}$, $\mathrm{d}\mathbf{S}$ is a differential area vector, normal to the face f_k and $\mathrm{d}V$ is a differential volume element. Defining the volumetric flux through a face as $q_{\mathsf{f}_k} = -\int_{\mathsf{f}_k}\mathbf{K}\cdot\boldsymbol{\nabla}P\cdot\mathrm{d}\mathbf{S}$ and the integrated source term as $F_\mathsf{p} = \int_{\mathcal{V}_\mathsf{p}} f\,\mathrm{d}V$, the previous equation can be written in a compact form as

$$\sum_{k=1}^{N_f} q_{\mathsf{f}_k} = F_\mathsf{p}\,. \tag{3}$$

After approximating fluxes through all the faces of the control volume $\mathcal{V}_\mathsf{p}$, and then substituting these expressions in Eq. (3), the discretized equation for this control volume is obtained. This equation, in the usual form of the finite volume method, can be written as

$$A_\mathsf{p}\,P_\mathsf{p} + \sum_{k=1}^{N_c} A_{\mathsf{n}_k} P_{\mathsf{n}_k} = b_\mathsf{p}\,, \tag{4}$$

where A_p e P_p are the coefficient and the pressure value associated with the cell p that coincides with the control volume $\mathcal{V}_\mathsf{p}$, while A_{n_k} and P_{n_k}, for $k = 1, 2, \ldots, N_c$, are the coefficients and pressure values associated with neighbor cells. It will be shown in the following section that, when using the CTPFA scheme, the stencil of the discretized equation includes only cells that share faces with the central cell.

2 CORRECTED TWO-POINT FLUX APPROXIMATION (CTPFA)

This scheme is applied in a conventional cell-centered finite volume method in polygonal (2D) or polyhedral grids (3D), where the control volumes are coincident with polygonal or polyhedral cells, respectively. It is an extension of the method originally proposed

in Mathur and Murthy (1997) as a part of a formulation for solving the Navies-Stokes equations. The CTPFA was developed introducing some alterations, in order to allow the adequate treatment of a flow in an anisotropic media.

The distinctive feature of the proposed scheme is that the discrete flux expressions are split into two terms. The first one involves only two values, corresponding to the two neighboring cells of a face, as is done in the conventional methods used in reservoir simulation. This term is treated implicitly, so it actually contributes to the coefficients of the discretized equation. The second term is a correction term that takes into account the influence of anisotropy and non-orthogonality, and involves a large set of points. Because of this, that term is expressed using pressure gradients approximated explicitly. In this way, the correction term will contribute only to the independent term of the discretized equation.

2.1 Derivation of the flux approximation

A semi-implicit approximation of diffusive fluxes on generic grids was proposed in Mathur and Murthy (1997), as a part of a formulation for the Navier-Stokes equations. The flux expression has the generic form

$$q_{\mathsf{f}} \approx T_{\mathsf{f}} \left(P_{\mathsf{p}} - P_{\mathsf{q}}\right) + Q_{\mathsf{f}}^{*}, \tag{5}$$

in which, in the context of our formulation, P_{p} and P_{q} would be the pressure values associated with the cells that share the face f. The coefficient T_{f} depends only on the geometry and Q_{f}^{*} is an explicit correction term that takes into account the non-orthogonality. If the grid is orthogonal, the correction term will be zero. It could be also understood as a transverse component of the diffusive flux.

A flux approximation of the form of Eq. (5) will be considered also in this work. However, the influence of an anisotropic and possibly heterogeneous permeability tensor will be introduced, since it is an important feature in reservoir flow models. The mathematical expression for that approximation will be derived in this section, following the development described originally in Maliska et al. (2012a). The configuration depicted in Fig. 2 will be considered in the derivation, in which an internal face f is shared by two polyhedral cells, p and q, each one with a specific permeability tensor associated. The vector $\Delta\mathbf{S}_{\mathsf{f}}$ is an orthogonal vector to the face f with modulus equal to area of the face.

At first, the approximation of the flux through face f will be considered only on the side of cell p. In order to do this, it is convenient to define the auxiliary vector

$$\boldsymbol{\sigma}_{\mathsf{f,p}} = \mathbf{K}_{\mathsf{p}} \cdot \Delta\mathbf{S}_{\mathsf{f}}, \tag{6}$$

resulting from the product of the permeability tensor and the face area vector. Since the permeability tensor is positive-definite, the $\boldsymbol{\sigma}_{\mathsf{f,p}}$ vector will always point to the same side than the face area vector.

The flux q_{f} can be expressed using vector $\boldsymbol{\sigma}_{\mathsf{f,p}}$ as follows

$$\begin{aligned} q_{\mathsf{f}} &= -\left[\mathbf{K}_{\mathsf{p}} \cdot (\boldsymbol{\nabla} P)_{\mathsf{p}}\right] \cdot \Delta\mathbf{S}_{\mathsf{f}} = -\Delta\mathbf{S}_{\mathsf{f}} \cdot \mathbf{K}_{\mathsf{p}} \cdot (\boldsymbol{\nabla} P)_{\mathsf{p}} = -\left[\mathbf{K}_{\mathsf{p}} \cdot \Delta\mathbf{S}_{\mathsf{f}}\right] \cdot (\boldsymbol{\nabla} P)_{\mathsf{p}} \\ &= -\boldsymbol{\sigma}_{\mathsf{f,p}} \cdot (\boldsymbol{\nabla} P)_{\mathsf{p}}, \end{aligned} \tag{7}$$

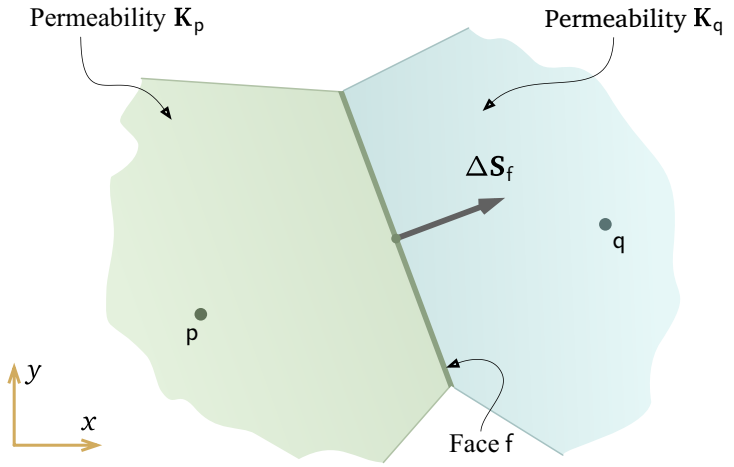

Figure 2: Entities involved in the approximation of the flux crossing the face f. Modified from Maliska et al. (2012b).

using the commutative property of the dot product and the fact that the permeability tensor is symmetrical. In the previous expression, $(\boldsymbol{\nabla} P)_\mathsf{p}$ is the mean value of pressure gradient on cell p.

The flux expression in Eq. (7) can be written in the alternative form

$$q_\mathsf{f} = -|\boldsymbol{\sigma}_{\mathsf{f,p}}|(\boldsymbol{\nabla} P)_\mathsf{p} \cdot \mathbf{e}_\sigma \,, \tag{8}$$

where $|\boldsymbol{\sigma}_{\mathsf{f,p}}|$ is the modulus of $\boldsymbol{\sigma}_{\mathsf{f,p}}$ and $\mathbf{e}_\sigma$ is the unit vector in the direction of $\boldsymbol{\sigma}_{\mathsf{f,p}}$. The equation (8) shows that in order to approximate the flux it is only needed the component of $(\boldsymbol{\nabla} P)_\mathsf{p}$ in the direction of $\mathbf{e}_\sigma$ or, in other words, the pressure derivative $(\partial_\sigma P)_\mathsf{p}$, along that direction.

Unfortunately, there is not a simple way of approximating the derivative $(\partial_\sigma P)_\mathsf{p}$. However, an expression of the form of Eq. (5) can be easily obtained if an auxiliary decomposition of the pressure gradient is introduced. In order to do that, let $\mathbf{e}_\xi$ be the unit vector in the direction of the line connecting the centroid of cell p and the centroid c of face f, as depicted in Fig. 3. A simple algebraic manipulation allows to decompose the pressure gradient in the flux expression in Eq. (8), introducing the unit vector $\mathbf{e}_\xi$, as shown next

$$\begin{aligned} q_\mathsf{f} &= -|\boldsymbol{\sigma}_{\mathsf{f,p}}|(\boldsymbol{\nabla} P)_\mathsf{p} \cdot \left(\mathbf{e}_\sigma + \mathbf{e}_\xi - \mathbf{e}_\xi\right) \\ &= -|\boldsymbol{\sigma}_{\mathsf{f,p}}|(\boldsymbol{\nabla} P)_\mathsf{p} \cdot \mathbf{e}_\xi - |\boldsymbol{\sigma}_{\mathsf{f,p}}|(\boldsymbol{\nabla} P)_\mathsf{p} \cdot \left(\mathbf{e}_\sigma - \mathbf{e}_\xi\right) . \end{aligned} \tag{9}$$

The unit vectors that appear in Eq. (9) can be easily determined by means of

$$\mathbf{e}_\sigma = \frac{\boldsymbol{\sigma}_{\mathsf{f,p}}}{|\boldsymbol{\sigma}_{\mathsf{f,p}}|} , \tag{10}$$

and

$$\mathbf{e}_\xi = \frac{\Delta\mathbf{r}_{\mathsf{pc}}}{|\Delta\mathbf{r}_{\mathsf{pc}}|} , \tag{11}$$

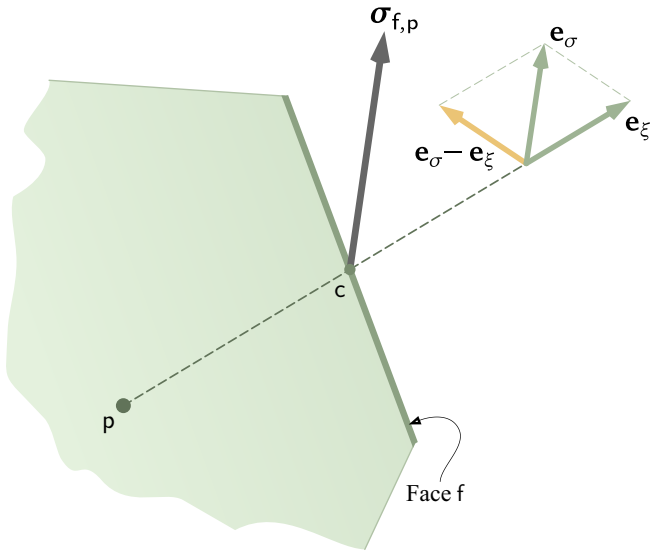

Figure 3: Geometrical entities associated with the cell p. Extracted from Maliska et al. (2012a).

respectively. In Eq. (11), $\Delta\mathbf{r}_{\mathrm{pc}} = \mathbf{r}_{\mathrm{c}} - \mathbf{r}_{\mathrm{p}}$ is the vector that connects the cell and the face centroids.

The remarkable feature on the flux expression in Eq. (9) is that a simple finite differences approximation can be used in the first term. That is

$$(\boldsymbol{\nabla} P)_{\mathrm{p}} \cdot \mathbf{e}_\xi = (\partial_\xi P)_{\mathrm{p}} \approx \frac{P_{\mathrm{c}} - P_{\mathrm{p}}}{\Delta\ell_{\mathrm{pc}}}, \tag{12}$$

where $\Delta\ell_{\mathrm{pc}} = |\Delta\mathbf{r}_{\mathrm{pc}}|$ is the distance between the cell and the face centroids. Later, the introduction of that approximation in Eq. (12) will lead to the two-point term in the final CTPFA expression.

Replacing the expressions on equations (10), (11) and (12) in Eq. (9), one obtains

$$q_{\mathrm{f}} \approx -|\boldsymbol{\sigma}_{\mathrm{f,p}}| \frac{P_{\mathrm{c}} - P_{\mathrm{p}}}{\Delta\ell_{\mathrm{pc}}} - |\boldsymbol{\sigma}_{\mathrm{f,p}}| (\boldsymbol{\nabla} P)_{\mathrm{p}} \cdot \left(\frac{\boldsymbol{\sigma}_{\mathrm{f,p}}}{|\boldsymbol{\sigma}_{\mathrm{f,p}}|} - \frac{\Delta\mathbf{r}_{\mathrm{pc}}}{|\Delta\mathbf{r}_{\mathrm{pc}}|} \right). \tag{13}$$

This last expression can be written in a more convenient compact way as

$$q_{\mathrm{f}} \approx \frac{P_{\mathrm{p}} - P_{\mathrm{c}}}{\nu_{\mathrm{f,p}}} + \Gamma^*_{\mathrm{f,p}}, \tag{14}$$

defining two new flux parameters, respectively, as

$$\nu_{\mathrm{f,p}} = \frac{\Delta\ell_{\mathrm{pc}}}{|\boldsymbol{\sigma}_{\mathrm{f,p}}|}, \tag{15}$$

$$\Gamma^*_{\mathrm{f,p}} = -|\boldsymbol{\sigma}_{\mathrm{f,p}}| (\boldsymbol{\nabla} P)^*_{\mathrm{p}} \cdot \left(\frac{\boldsymbol{\sigma}_{\mathrm{f,p}}}{|\boldsymbol{\sigma}_{\mathrm{f,p}}|} - \frac{\Delta\mathbf{r}_{\mathrm{pc}}}{|\Delta\mathbf{r}_{\mathrm{pc}}|} \right). \tag{16}$$

It is assumed in Eq. (16) that the mean pressure gradient in cell p, $(\boldsymbol{\nabla} P)^*_{\mathrm{p}}$, is approximated explicitly by a gradient reconstruction method. The asterisk notation is used to point

out that approximation is made using pressure values from a previous iterative level. Consequently, it is assumed also that the numerical solution is obtained by means of an iterative process. The gradient reconstruction method employed in this work is described briefly in the next section.

A similar derivation can be made considering the side of cell q, the other cell that shares face f. That derivation leads to the expression

$$q_{\mathsf{f}} \approx \frac{P_{\mathsf{c}} - P_{\mathsf{q}}}{\nu_{\mathsf{f,q}}} + \Gamma^*_{\mathsf{f,q}}, \tag{17}$$

where the $\nu_{\mathsf{f,q}}$ and $\Gamma^*_{\mathsf{f,q}}$ parameters are defined by expressions similar to Eqs. (15) and (16), respectively. As a matter of fact, it is only necessary to write index q instead of index p in those equations in order to obtain the correspondent expressions.

Equations (14) and (17) can be manipulated algebraically in order to eliminate P_{c}, the pressure value at the face centroid. After doing that, the resulting flux expression includes only the pressure values at the centroids of the two neighbor cells

$$q_{\mathsf{f}} \approx \frac{P_{\mathsf{p}} - P_{\mathsf{q}}}{\nu_{\mathsf{f,p}} + \nu_{\mathsf{f,q}}} + \frac{\nu_{\mathsf{f,p}}\Gamma^*_{\mathsf{f,p}} + \nu_{\mathsf{f,q}}\Gamma^*_{\mathsf{f,q}}}{\nu_{\mathsf{f,p}} + \nu_{\mathsf{f,q}}}. \tag{18}$$

This last expression can be cast into the form of Eq. (5) defining the transmissibility coefficient T_{f} and correction term Q^*_{f}, respectively, as

$$T_{\mathsf{f}} = \frac{1}{\nu_{\mathsf{f,p}} + \nu_{\mathsf{f,q}}}, \tag{19}$$

$$Q^*_{\mathsf{f}} = \frac{\nu_{\mathsf{f,p}}\Gamma^*_{\mathsf{f,p}} + \nu_{\mathsf{f,q}}\Gamma^*_{\mathsf{f,q}}}{\nu_{\mathsf{f,p}} + \nu_{\mathsf{f,q}}}. \tag{20}$$

The expression in Eq. (18) defines the CTPFA scheme used in this work. As mentioned previously, two terms form part of the approximation. The first one including only two discrete pressure values, which is treated implicitly, and a correction term that is considered explicitly in the formulation. The correction term will be zero only in an isotropic problem solved in a locally orthogonal grid. In any other case, its value will be computed explicitly, because it depends on pressure gradients, whose approximation is always a complex process in a generic grid. The drawback of this approach is that the solution process of the discrete equations must be iterative, since the correction terms must be updated until pressure gradients stop changing.

A direct consequence of the explicit treatment of correction terms is that stencil of a discretized equations remain compact. Since in the CTPFA expression only pressures at the cells that share a face remain as active variables, the stencil after assembling the discretized equation for a cell will include only neighbor cells that share a face. This is depicted in Fig. 4, for a polygonal grid (for ease of visualization). The configuration is similar for theedimensional polyhedral grids.

An important property of the scheme just derived is that it leads to a positive-coefficient discretized equation, after substituting the flux expressions into the balance equation for a

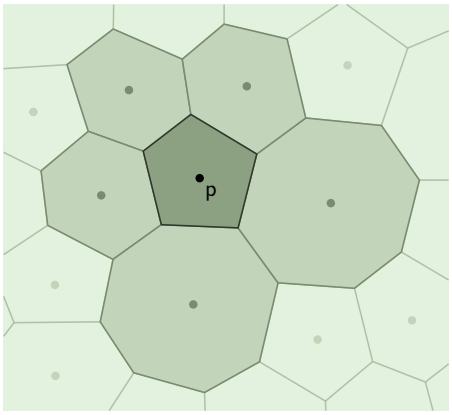

Figure 4: Stencil of the discretized equation related to the cell p. Modified from Maliska et al. (2012b).

control volume. A sufficient condition for satisfying that property is that all transmissibility coefficients T_f remain positive. Equation (19) shows that is sufficient that both parameters $\nu_{f,p}$ and $\nu_{f,q}$ be positive in order to assure the positivity of T_f. And since both parameters are the quotient of two always positive parameters, as shown in Eq. (15), the positive-coefficient condition is assured with the CTPFA scheme previously derived.

2.2 Gradient reconstruction

As previously mentioned, in order to approximate the flux through a face using CTPFA, mean values of pressure gradients in cells are needed for the correction term. Those gradients can be determined using the so-called gradient reconstruction methods. Its only purpose is to approximate gradient vectors employing a reduced set of discrete values of a scalar variable, the pressure in the present case. Since a cell-center method is considered here, the discrete pressure values must be associated with cell centroids. It is important to notice that, in the scheme considered here, those values are already available, since they are related to a previous iterative level. The schematic process of gradient reconstruction is illustrated in Fig. 5.

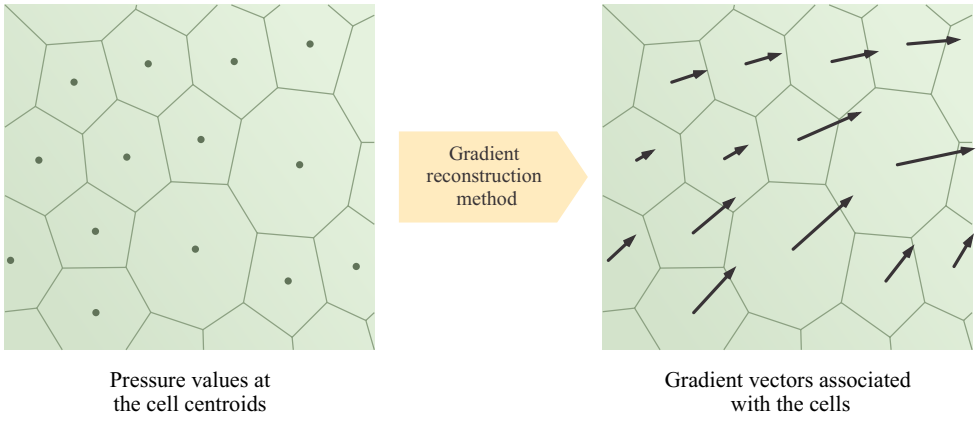

Figure 5: Application of a gradient reconstruction method in a polygonal grid. Modified from Maliska et al. (2012b).

Several gradient reconstruction methods are described in the literature. Some of them employ the Green-Gauss formula, derived from the divergence theorem, while others transform the gradient reconstruction problem into a least squares problem (Mathur and Murthy, 1997, Lee et al., 2010, Correa et al., 2011). An extensive comparative study made in Maliska et al. (2012a) concluded that methods based on least squares are more robust and accurate, specially when dealing with very distorted grids. Furthermore, they can be efficiently implemented in a computational code, leading to comparatively smaller computational times (Cerbato, 2012). For those reasons, a least squares reconstruction method was chosen in this work for complementing the CTPFA scheme.

In order to derive the least squares problem associated to the gradient approximation, a linear variation of the scalar variable in the vicinity of a generic cell p is considered. A truncated Taylor series expansion around the centroid of that cell leads to the following expression for the pressure at the center point of a neighbor cell n_k

$$P_{\mathsf{n}_k} \approx P_{\mathsf{p}} + (\boldsymbol{\nabla} P)_{\mathsf{p}} \cdot \Delta \mathbf{r}_{\mathsf{p},\mathsf{n}_k}\,, \tag{21}$$

where $\Delta \mathbf{r}_{\mathsf{p},\mathsf{n}_k}$ is the vector that connects the centroids of cells p and n_k, whereas $(\boldsymbol{\nabla} P)_{\mathsf{p}}$ is the pressure gradient associated with cell p.

Equation (21) can be particularized for all neighbor cells around cell p. The only unknowns in all resulting equations are the components of the gradient in cell p, $(\boldsymbol{\nabla} P)_{\mathsf{p}} = (\partial_x P, \partial_y P, \partial_z P)_{\mathsf{p}}$. After multiplying each equation by a weighting factor, the following system of linear equations can be written

$$\begin{pmatrix} w_1 \Delta x_1 & w_1 \Delta y_1 & w_1 \Delta z_1 \\ w_2 \Delta x_2 & w_2 \Delta y_2 & w_2 \Delta z_2 \\ \vdots & \vdots & \vdots \\ w_m \Delta x_m & w_m \Delta y_m & w_m \Delta z_m \end{pmatrix} \begin{pmatrix} \partial_x P \\ \partial_y P \\ \partial_z P \end{pmatrix}_{\mathsf{p}} = \begin{pmatrix} w_1 (P_{\mathsf{n}_1} - P_{\mathsf{p}}) \\ w_2 (P_{\mathsf{n}_2} - P_{\mathsf{p}}) \\ \vdots \\ w_m (P_{\mathsf{n}_m} - P_{\mathsf{p}}) \end{pmatrix} \tag{22}$$

where Δx_k, Δy_k, Δz_k, for $k = 1, \ldots, m$, are the cartesian components of the vector $\Delta \mathbf{r}_{\mathsf{p},\mathsf{n}_k}$, while $m = N_c$ is the number of neighbor cells of p and w_k are the referred weighting factors. Those factors w_k are usually related to geometric parameters. In the present work an inverse square distance weighting was considered.

In general, $m > 3$ for a polyhedral grid, consequently the linear system in Eq. (22) will be overdetermined. It only can be obtained a solution in the sense of a least squares problem. This problem can be solved using different techniques (Demmel, 1997, Strang, 1988). For obtaining the results presented in the following section, a QR factorization was employed in order to solve the least squares problem.

3 RESULTS

Some results of a problem test employing the CTPFA formulation are presented in this section. The performance of the proposed methodology is evaluated taking into account two factors: the anisotropy of permeability and the grid distortion. The analysis will focus on the reduction of the error associated to both the pressure and its gradient.

3.1 Problem specification

In the problem test, the single-phase flow equation defined in section 1.2 is solved in the unit cube domain shown in Fig. 6. As mentioned before, one of the aspects to be analyzed is the influence of permeability anisotropy on the performance of the CTPFA scheme. In order to control the degree of anisotropy and the orientation of the principal axes of the permeability tensor, the following expression will be considered

$$\mathbf{K} = \mathbf{Q}\check{\mathbf{K}}\mathbf{Q}^{\mathsf{T}}, \tag{23}$$

where $\check{\mathbf{K}}$ is the diagonal tensor

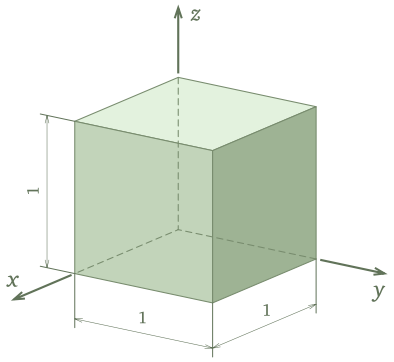

Figure 6: Problem domain.

$$\check{\mathbf{K}} = \begin{pmatrix} 1 & 0 & 0 \\ 0 & 1 & 0 \\ 0 & 0 & R \end{pmatrix}, \tag{24}$$

and $\mathbf{Q}$ is the rotation matrix

$$\mathbf{Q} = \begin{pmatrix} \cos\gamma & \sin\beta\sin\gamma & \cos\beta\sin\gamma \\ 0 & \cos\beta & -\sin\beta \\ -\sin\gamma & \sin\beta\cos\gamma & \cos\beta\cos\gamma \end{pmatrix}. \tag{25}$$

Equation (23) gives the components in Cartesian coordinates of a tensor of principal values $\{1,1,R\}$ whose principal axes are rotated an angle β around the x axis and an angle γ around the y axis. In that way, the parameter R can be interpreted as an anisotropy ratio. Four typical values were considered in the tests, $R = \{1, 10, 100, 1000\}$, where $R = 1$ corresponds to the isotropic case. In order to examine the influence of permeability principal directions, different values for the angles β and γ were considered also in some tests.

The so-called *method of the manufactured solutions* (Salari and Knupp, 2000) was chosen in order to analyze the numerical errors associated to the proposed formulation. In that method, a given function is chosen as the analytical solution of a differential equation. The source term of the equation is then determined from the condition that the function must

satisfy identically the differential equation. In the present case, the following function was selected as the analytical solution of Eq. (1)

$$P^{\text{an}}(x,y,z) = 5x - 3y + 2z + 2\,\sin(7x+1)\sin(4y+1)\sin(2z+1)\,. \tag{26}$$

The correspondent source term f is determined replacing the function in Eq. (26) and the permeability tensor computed by Eq. (23) into Eq. (1). In order to obtain the numerical solution, Dirichlet conditions are considered on all boundaries, with pressure values given also by Eq. (26).

3.2 Grids considered

Five sets of polyhedral grids were used in the tests. Each set is formed for six grids with the same logical structure and distortion type but different refinement level. Almost all those sets are based on the grids of the first set, which are called here as regular (REG), because they where obtained as dual polyhedral grids of regular tetrahedral grids. The process of obtaining a polyhedral grid from a tetrahedral one is described in Maliska et al. (2011).

Three sets of distorted grids were obtained displacing the vertices on regular grids. The new vertex coordinates are computed by

$$\begin{cases} x'_{\text{v}} = x_{\text{v}} + \delta_x(x_{\text{v}}, y_{\text{v}}, z_{\text{v}})\,, \\ y'_{\text{v}} = y_{\text{v}} + \delta_y(x_{\text{v}}, y_{\text{v}}, z_{\text{v}})\,, \\ z'_{\text{v}} = z_{\text{v}} + \delta_z(x_{\text{v}}, y_{\text{v}}, z_{\text{v}})\,, \end{cases} \tag{27}$$

in which x_{v}, y_{v} and z_{v} are the original vertex coordinates in a regular grid. Each set of distorted grids is characterized by given displacement functions δ_x, δ_y and δ_z. Those sets of distorted grids are named here as sinusoidal (SIN), random (RAN) and stripped (STP). In the grids with sinusoidal distortion, all displacements are equal at a vertex and given by a product of sinusoidal functions of the vertex coordinates. In the RAN grids, vertex displacements are given by random values bounded by a given maximum amplitude. In the STP grids, displacements in each direction are given by different sinusoidal functions, resulting grids with alternate strips of wide and narrow cells. A forth set of distorted grids is formed by stretched grids (STC), which come from tetrahedral regular grids in which all cells were stretched in a given direction. Cells in that set have an aspect ratio of approximately 10:1. A grid of each set is shown in Fig. 7.

As mentioned before, each set of grids is composed by six grids of different refinement level. In four sets (REG, SIN, RAN and STP) the coarsest grid has 189 cells, whereas the most refined has 242649 cells. In the case of the stretched grid set (STC), the coarsest grid has 11389 cells and the most refined one has 263395.

In order to characterize the convergence rate of the numerical scheme, it is necessary to attribute a characteristic length to every grid. The following expression was considered here for estimating such parameter

$$h = \frac{1}{N_c(\Omega)} \sum_{k=1}^{N_c(\Omega)} (\Delta V_k)^{1/3}\,, \tag{28}$$

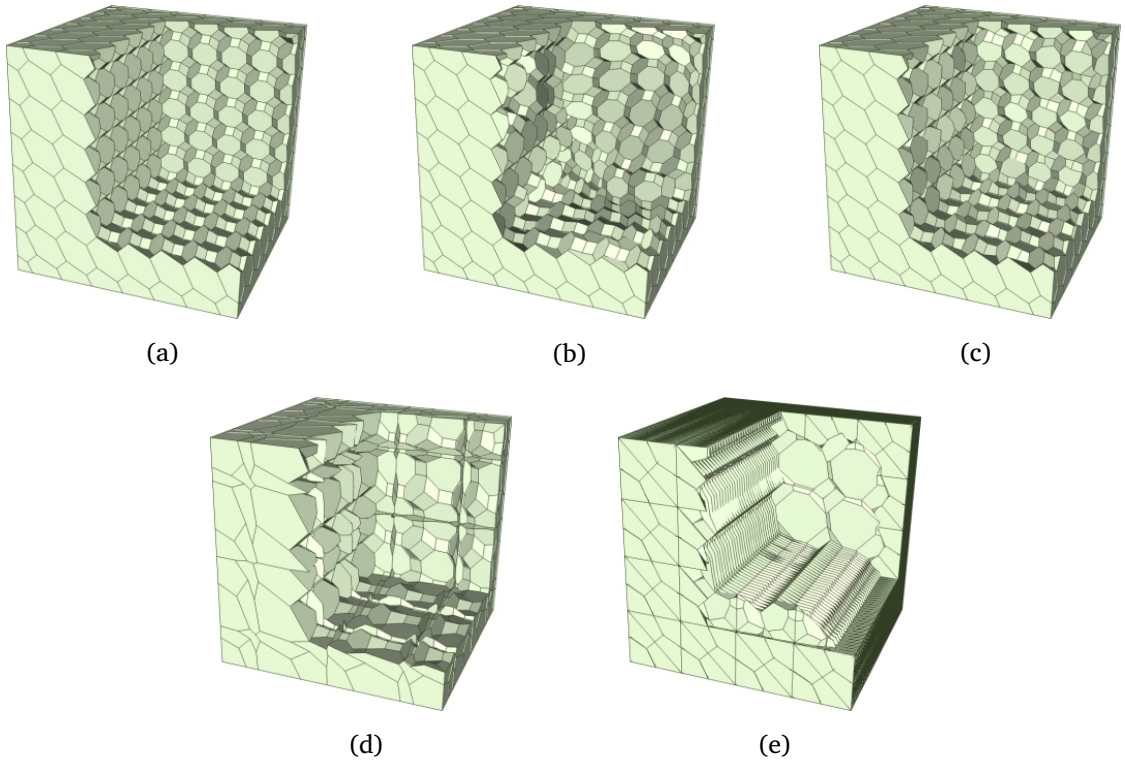

Figure 7: Examples of grids used in the tests: (a) REG – regular, (b) SIN – sinusoidal distortion, (c) RAN – random distortion, (d) STP – stripped distortion, (e) STC – stretched distortion.

where $N_c(\Omega)$ is the number of cells in the grid and ΔV_k is the volume of each cell k. The characteristic length of each cell is considered to be the cubic root of its volume. Therefore, Eq. (28) defines the characteristic length for a grid as the arithmetic mean of the characteristic lengths of its cells.

3.3 Error estimation

Most of the performance analysis of the CTPFA formulation will be based on the behavior of the error associated to the numerical solution. At a centroid of a cell of the grid, the error on the pressure field can be defined as

$$(\epsilon_P)_{\mathrm{c}_k} = P^{\mathrm{an}}_{\mathring{\mathrm{c}}_k} - P^{\mathrm{nu}}_{\mathrm{c}_k}, \tag{29}$$

where $P^{\mathrm{an}}_{\mathring{\mathrm{c}}_k}$ is the analytical solution evaluated at the centroid of cell k and $P^{\mathrm{nu}}_{\mathrm{c}_k}$ is the discrete value of pressure on the numerical solution, associated also to the centroid of the referred cell. Similarly, the error on the pressure gradient was defined as

$$(\epsilon_{\nabla P})_{\mathrm{c}_k} = \left| (\boldsymbol{\nabla} P)^{\mathrm{an}}_{\mathring{\mathrm{c}}_k} - (\boldsymbol{\nabla} P)^{\mathrm{nu}}_{\mathrm{c}_k} \right|. \tag{30}$$

where $(\boldsymbol{\nabla} P)^{\mathrm{an}}_{\mathring{\mathrm{c}}_k}$ is the analytical gradient vector, evaluated at the centroid of cell k and $(\boldsymbol{\nabla} P)^{\mathrm{nu}}_{\mathrm{c}_k}$ is the mean pressure gradient vector associated to the same cell, computed by means of the gradient reconstruction procedure outlined in section 2.2.

In order to characterize the error associated to a given grid by a single value, frequently the L_2-norm of the error is considered. The following norm is considered here

$$\|\epsilon_P\|_2 \approx \left[\frac{\sum_{k=1}^{N_c(\Omega)} \left(P^{\mathrm{nu}}_{\mathrm{c}_k} - P^{\mathrm{an}}_{\mathring{\mathrm{c}}_k} \right)^2 \Delta V_k}{\sum_{k=1}^{N_c(\Omega)} \left(P^{\mathrm{an}}_{\mathring{\mathrm{c}}_k} \right)^2 \Delta V_k} \right]^{1/2} . \tag{31}$$

Note that the numerator of the Eq. (31) is the sum of squares of cell pressure errors and the denominator has the role of a normalization parameter. As for the norm of the error on the pressure gradient, the following expression was considered

$$\|\epsilon_{\nabla P}\|_2 \approx \left(\frac{\sum_{k=1}^{N_c(\Omega)} \left| (\boldsymbol{\nabla} P)^{\mathrm{nu}}_{\mathrm{c}_k} - (\boldsymbol{\nabla} P)^{\mathrm{an}}_{\mathring{\mathrm{c}}_k} \right|^2 \Delta V_k}{\sum_{k=1}^{N_c(\Omega)} \left| (\boldsymbol{\nabla} P)^{\mathrm{an}}_{\mathring{\mathrm{c}}_k} \right|^2 \Delta V_k} \right)^{1/2} . \tag{32}$$

3.4 Details of the solution process

As mentioned before, in order to solve the fluid flow model considered here it is needed to use an iterative process of gradient updating for the explicit term of the flux approximation. The process begins from a zero pressure field and goes until the following stop criterion is reached

$$\frac{\| \mathbf{P}^n - \mathbf{P}^{n-1} \|_\infty}{\| \mathbf{P}^n \|_\infty} < \mathrm{TOL}_{\mathrm{ite}} . \tag{33}$$

in which $\mathbf{P}^n$ and $\mathbf{P}^{n-1}$ are two consecutive pressure fields in the iterative process, while $\mathrm{TOL}_{\mathrm{ite}}$ is a user-specified value. After several numerical experiments, 10^{-5} was chosen as an adequate value for $\mathrm{TOL}_{\mathrm{ite}}$. At each iteration, a linear system of equations is assembled and solved, as described in previous sections, in order to obtain a new discrete pressure field. The system of linear equations was solved using the additive correction multigrid method implemented in the ACMLib library (Maliska et al., 2010), with a specified tolerance of 10^{-4}.

3.5 Analysis of the influence of permeability anisotropy

Two aspects of an anisotropic permeability tensor can influence the behavior of a numerical method. One of them is the anisotropy strength, which can be characterized by the parameter R in Eq. (24). The other aspect is the orientation of the principal direction of the permeability tensor, which are determined indirectly by angles β and γ in the rotation matrix defined in Eq. (25).

Influence of anisotropy ratio. The purpose of the analysis here is to determine how sensitive the numerical error is to the increasing of permeability ratio R. The results presented in Figs. 8 and 9 were obtained using the set of grids with sinusoidal distortion (SIN). For that specific test, the permeability principal directions were kept fixed, setting $\beta = 60^o$ and $\gamma = 75^o$, whereas the anisotropy ratio was increased from $R = 1$ (the isotropic case) up to $R = 1000$.

The graph in Fig. 8 illustrates the reduction of the norm of pressure error as grids are refined. Each point in that graph corresponds to a given grid in the set and a given value of

R. Along with those points, the graphs displays also trend lines obtained fitting the points to curves of the form $\|\epsilon_P\|_2 = ah^b$. In that way, the exponent b can be considered an estimate of the convergence rate of the pressure, for a given anisotropy ratio. As can be seen in Fig. 8, the convergence rate is near second order in the isotropic case ($R = 1$). Convergence rate degrades to some extent as the anisotropy ratio increases, specially when going from $R = 1$ to $R = 10$ and from $R = 10$ to $R = 100$. On the other hand, little difference exists between correspondent error values for $R = 100$ and $R = 1000$. A similar behavior was observed in other grid sets and different principal directions.

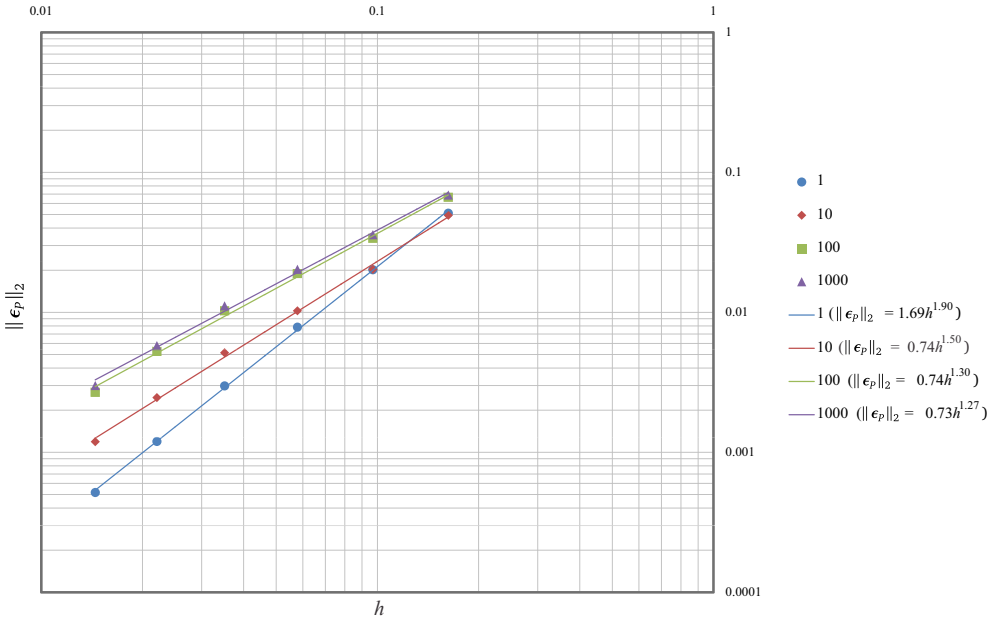

Figure 8: Convergence of pressure for different anisotropy ratios.

The graph in Fig. 9 displays the behavior of the norm of error in pressure gradient. That behavior is qualitatively similar to the one already seen for the norm of pressure error in Fig. 8. However, some differences can be noticed. First, actual values of the norm of error on gradients are approximately one order of magnitude bigger than the correspondent to the norm of pressure error. On the other hand, maximum convergence rate for the gradient error is lower, near to 1.5 for the isotropic case. Convergence rate decay is somewhat less pronounced, though.

A phenomenon worth of mention was observed during the execution of tests increasing the anisotropy ratio. The number of iterations needed to attain a given convergence level was strongly dependent on the anisotropy ratio. As the value of R was increased, more iterations were needed to reach the stop criterion specified in Eq. (33). For instance, when the most refined grid in the set was used, convergence were reached after 34 iterations for $R = 1$. But when R was increased to 10, the number of iteration grew to 41. Furthermore, for $R = 100$, the number of iterations grew to 65. Consequently, the convergence of the proposed scheme becomes more difficult as the anisotropy level increases.

Influence of the orientation of principal axes. In the previous analysis, anisotropy ratio was varied while permeability principal directions were kept fixed. Now, the opposite situation is considered. Anisotropy ratio is fixed at $R = 1000$, while different combinations of

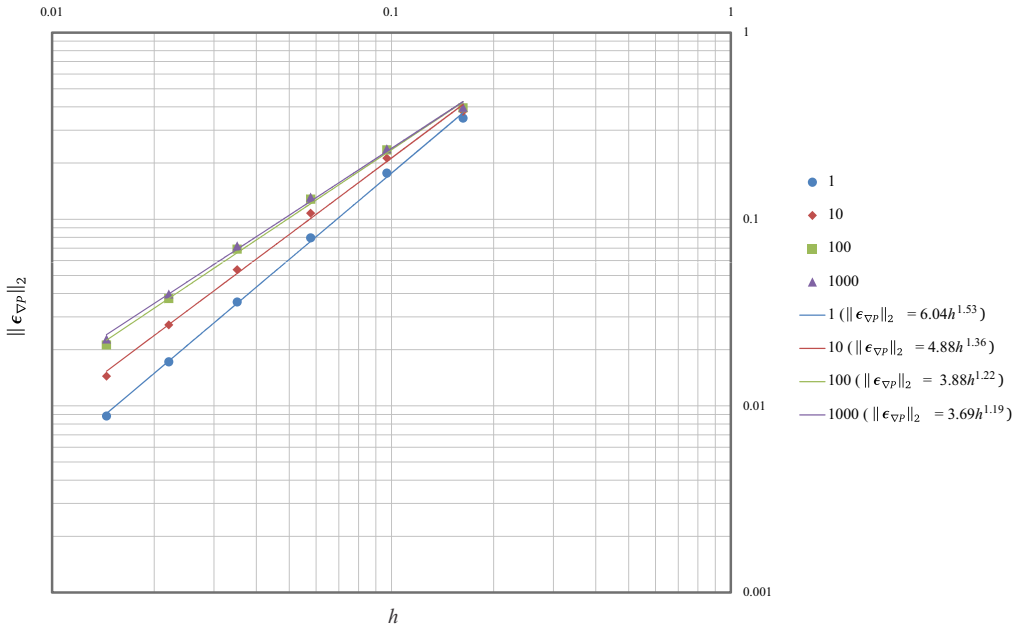

Figure 9: Convergence of pressure gradient for different anisotropy ratios.

β and γ angles are considered. The graph in Fig. 10 shows the convergence of pressure for six different combinations: {75°, 0°}, {75°, 60°}, {75°, 120°}, {150°, 0°}, {150°, 60°} and {150°, 120°}. The set of grids with sinusoidal distortions was used again for that test. The graph in Fig. 10 suggests that the CTPFA formulation is equal or even more sensitive to the variation on the principal axes direction than to the anisotropy ratio, since a relatively wide variation of the convergence rate can be seen in that graph.

3.6 Analysis of the influence of grid distortions

The influence of grid distortions on the convergence of the CTFA formulation is the second aspect analysed in this paper. In order to do that, several tests were carried out using the five sets of grids described in section 3.2 and maintaining permeability fixed. For the results presented next, the permeability tensor was defined setting $R = 1000$, β =120° and γ =75°.

The convergence of pressure is shown in Fig. 11 for the different grid series. As would be expected, the lower values of the error norm correspond to the regular grids. Nevertheless, the values of the error norm for the randomly distorted grids (RAN) are very close to the correspondent to the regular ones. In order to avoid cell superposition, a very small amplitude was considered for the random vertex displacements and most probably that was the cause for the proximity between those values. The largest decrease on the convergence rate is observed for the grids with sinusoidal distortions (SIN). However, the bigger differences regarding the values of error norm are observed between those correspondent to the stretched grids (STC) and the rest. This suggest that the CTPFA formulation is most sensitive to the stretching of the cells than to other types of distortion.

Figure 12 shows the convergence of gradient pressure for the different set of grids considered. The behavior is roughly the same observed previously for the convergence of pressure. As before, however, the actual values of the error norm for the pressure gradient are

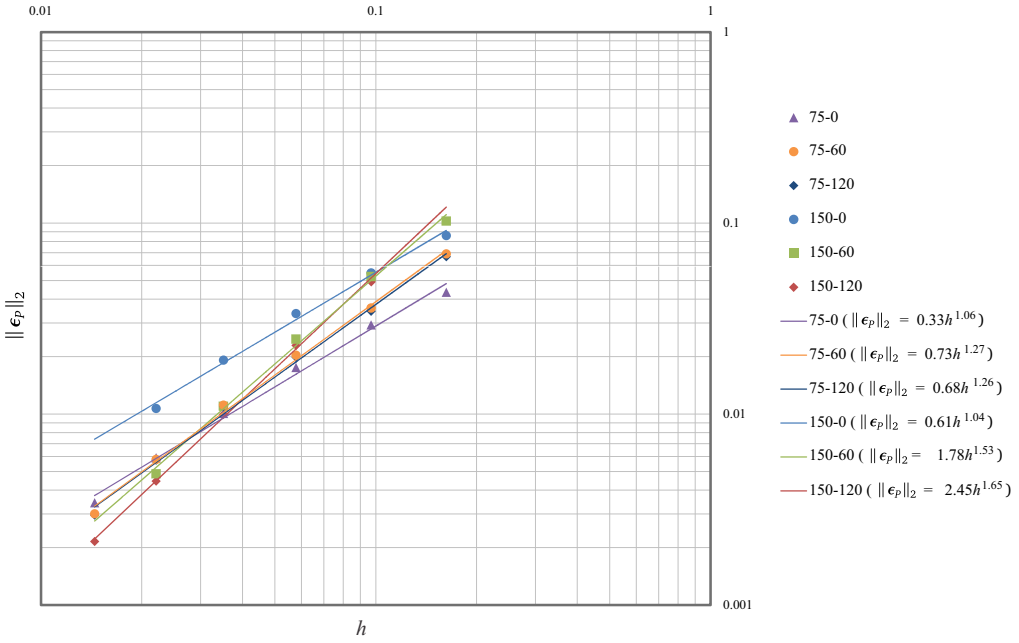

Figure 10: Pressure convergence for different orientations of principal directions of permeability tensor.

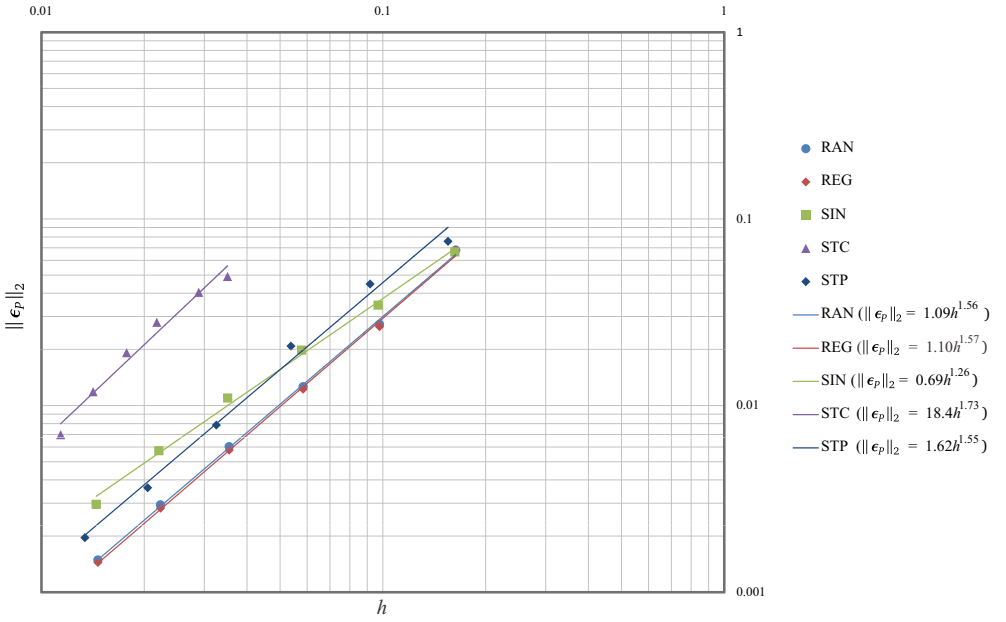

Figure 11: Convergence of pressure for different grid distortion types.

largest than for the pressure. The convergence rates for pressure gradient are slightly lower also.

It is noteworthy to mention that in some occasions the iterative process of solution in the CTPFA formulation fails to converge. There were observed cases for some specific combinations of grid distortions and permeability tensors in which the norm of the difference between consecutive pressure fields did not diminish at all during the iterative process. That situation was mostly observed when using the set of stretched grids. Several strategies were tested in order to address that issue, but none was successful when using the semi-implicit

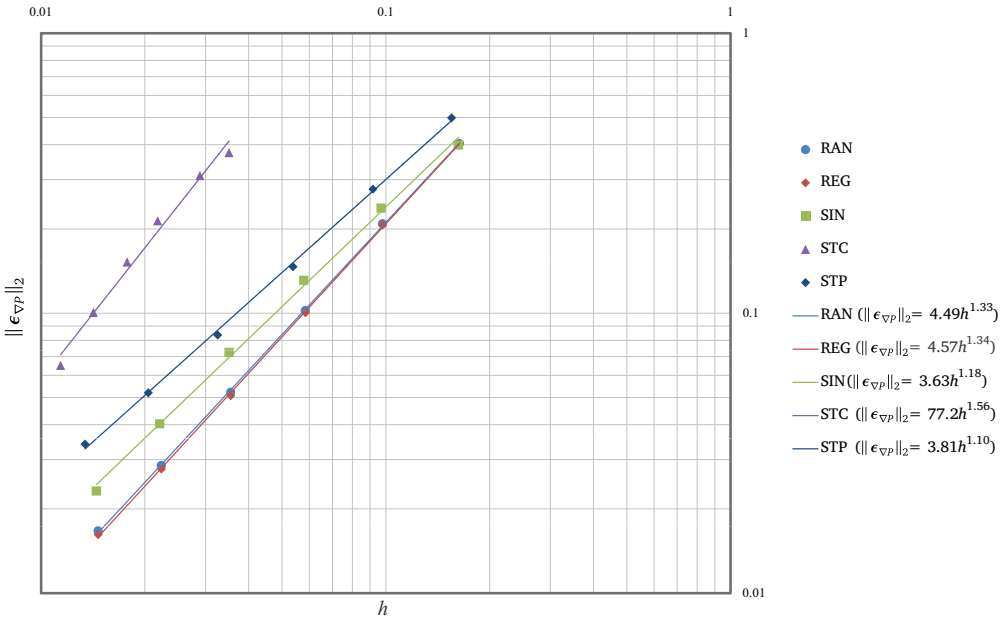

Figure 12: Convergence of pressure gradient for different grid distortion types.

flux approximation as proposed in this work.

The only alternative that permitted the obtention of a solution for all cases was one in which the correction term in the flux approximation is treated implicitly also. This implies that all pressure values in the flux approximation remains as active variables and, consequently, there is no more necessity of an iterative solution process. The main drawback of this approach is the significantly increase on the size of the stencil for a discretized equation. As a consequence, the methodology becomes more memory-demanding and the resulting linear system more difficult to solve. Nonetheless, as already mentioned, that was the only way in which the formulation was able to provide solutions for all combinations of grid distortion and permeability anisotropy.

4 CONCLUSIONS

A finite volume formulation for reservoir simulation suitable to deal with general polyhedral grids was proposed in this paper. The main feature of the formulation is the partially explicit approximation of the fluxes through control volume interfaces. The expression for approximating the fluxes is split into two terms, one dependent only on two pressure values and a second one, a correction term, that takes into account both non-orthogonality and anisotropy. Because of that, the scheme was named as *corrected two-point flux approximation* (CTPFA). The first term in the flux approximation is treated in implicit way, thus keeping the related two pressure discrete values as active variables. On the other hand, in order to maintaing simplicity, the second term is treated explicitly. Pressure gradients, needed for computing that correction term, are obtained by means of a gradient reconstruction procedure, using pressure values from a previous iteration. The major drawback of the formulation is the necessity of an iterative process in order to find a numerical solution for the pressure field, even when considering a linear flow model.

The proposed formulation was tested considering an incompressible single-phase flow model, in which only a pressure differential equation must be solved. The analysis of sensi-

tivity of the results to the permeability anisotropy and grid distortions was one of the main objectives of the tests. It was observed that in the more favorable situations, when the grid is only slightly distorted and the permeability is isotropic, the convergence rate of pressure is near second order. The increasing of permeability anisotropy and grid distortions cause an important reduction in the convergence rate and sometimes an increase of the error level.

One major drawback found when testing the formulation is a lack of robustness for more adverse cases with high permeability anisotropy and strong grid distortion. Even when the iterative process converges in such situations, the number of iterations to reach a certain convergence level grows significantly as the anisotropy ratio increases. One possible alternative to address that difficulty is the fully implicit treatment of the flux approximation. In that way there is no more necessity of an iterative solution process, since all pressure values remain as active variables in the flux approximation. The disadvantage of this approach is the considerable increase in the requirement of memory in order to assemble and solve the system of linear equations. In future works, that approach will be further studied and compared with the semi-implicit approach presented in this work.

PERMISSION

The authors are the only responsibles for the printed material included in this paper.

ACKNOWLEDGEMENTS

This work was supported by the MaTra Project, granted by the Reservoir Simulation and Management Network (SIGER) and Petrobras.

REFERENCES

Cerbato, G., 2012. Esquemas numéricos para a reconstrução do gradiente em malhas poligonais. Dissertação de mestrado, Departamento de Engenharia Mecânica, Universidade Federal de Santa Catarina, Florianópolis, Brasil.

Correa, C. D., Hero, R., and Ma, K.-L., 2011. A comparison of gradient estimation methods for volume rendering on unstructured meshes. *IEEE Transactions on Visualization and Computer Graphics*, 17(3):305–319.

Demmel, J. W., 1997. *Applied numerical linear algebra*. Society for Industrial and Applied Mathematics, Berkeley, California.

Lee, H., Jeong, J. J., Cho, H. K., and Yoon, H. Y., 2010. An improved numerical scheme to evaluate the pressure gradient on unstructured meshes for two-phase flow analysis. *International Communications in Heat and Mass Transfer*, 37:1273–1279.

Maliska, C. R., Silva, A. F. C., Hurtado, F. S. V., Donatti, C. N., and Pescador Jr., A. V. B., 2010. Desenvolvimento e implementação da biblioteca ACMLib. Relatório técnico SINMEC/SIGER I-04, parte 2, Departamento de Engenharia Mecânica, Universidade Federal de Santa Catarina.

Maliska, C. R., Silva, A. F. C., Hurtado, F. S. V., Pescador Jr., A. V. B., Ribeiro, G. G., Cerbato, G., and Grein, E. A., 2011. Estudos preliminares sobre malhas de transição. Relatório técnico SINMEC/SIGER I-07, Departamento de Engenharia Mecânica, Universidade Federal de Santa Catarina.

Maliska, C. R., Silva, A. F. C., Hurtado, F. S. V., Ribeiro, G. G., Cerbato, G., and Grein, E. A., 2012a. Implementação e experimentos numéricos com o método baseado na reconstrução do gradiente. Relatório técnico SINMEC/SIGER II-02, Departamento de Engenharia Mecânica, Universidade Federal de Santa Catarina.

Maliska, C. R., Silva, A. F. C., Hurtado, F. S. V., Ribeiro, G. G., Pescador Jr., A. V. B., Grein, E. A., and Cerbato, G., 2012b. Introdução às malhas poliédricas e ao método baseado na reconstrução explícita do gradiente. Relatório técnico SINMEC/SIGER II-01, Departamento de Engenharia Mecânica, Universidade Federal de Santa Catarina.

Mathur, S. R. and Murthy, J. Y., 1997. A pressure-based method for unstructured meshes. *Numerical Heat Transfer, Part B*, 31:195–215.

Salari, K. and Knupp, P., 2000. Code verification by the method of manufactured solutions. Report sand2000–1444, Sandia National Laboratories, Albuquerque, USA.

Strang, G., 1988. *Linear algebra and its applications*. Harcourt Brace Jovanovich Publishers, San Diego, USA, third edition edition.